# Supporting Information

# Ultrafast Propulsion of Water Nanodroplets

# on Patterned Graphene

Ermioni Papadopoulou,[†] Constantine M. Megaridis,[‡] Jens H. Walther,[†,¶] and

Petros Koumoutsakos[*,†]

[†]Computational Science and Engineering Laboratory, ETH Zürich, Zürich, CH-8092, Switzerland

[‡]Department of Mechanical and Industrial Engineering, University of Illinois at Chicago, Chicago, Illinois 60607, USA

[¶]Department of Mechanical Engineering, Technical University of Denmark, 2800 Kongens Lyngby, Denmark

E-mail: petros@ethz.ch

# 1 Methods

## 1.1 Droplet equilibration

The equilibration of the droplets before the production runs takes place in the NVT ensemble, over a surface with wettability that varies. The process starts with a water cubic volume placed on top of a graphene surface (GRS). The water molecules are assigned a velocity distribution corresponding to an average temperature value of 298 K and the system is let to equilibrate into the final shape of the droplet. We used a neutrally-wettable surface for the equilibration of the water droplets, resulting in a contact angle of the water droplet with the substrate equal to 90°.

## 1.2 Change of surface wettability

The surface wettability in this study is tuned by varying the strength of the non-bonded interaction between the oxygen and carbon atoms. The non-bonded interaction is modeled with a Lennard-Jones (LJ) 6-12 potential, therefore the interaction strength varies with the value of the LJ potential well, $\epsilon_{CO}$.

## 1.3 Effect of cutoff distance of short-range interactions

In the MD simulations, the non-electrostatic interactions are modelled as a Lennard-Jones potential for all interaction pairs of the system: the cut-off for the computation of the Lennard-Jones potential is set to 9 Å for Oxygen-Oxygen interaction, in order to account for the offset distance of the fictitious charges on O atoms in water molecules.[1] In turn, the Lennard-Jones cut-off for the Carbon-Oxygen interaction is set to 10 Å.[2] The non-bonded interaction between Carbon atoms is modelled as a Lennard-Jones potential as well, with a cut-off of 10 Å, although for the majority of simulations the carbon atoms remain rigid.

We perform a sensitivity analysis, modifying the number of computing cores employed for the MD simulations. We find that round-off and computational tolerances can vary the

calculated end-velocity of the water droplet by $\pm 7.5\%$. In order to check the sensitivity of our results to the selection of the potential cut-off distance, we performed simulations, varying the cut-off distance of the C-O Lennard-Jones interactions. We find that, increase of the cut-off distance of the C-O LJ interaction from 10 Å to 11 Å increases the maximum $V_{CoM}$ on average by 5.5%, whereas a 10% decrease of the cut-off distance of the C-O LJ interaction decreases the maximum $V_{CoM}$ of the water droplet by 4.0% on average. Lastly, we performed additional simulations, where the LJ interactions were shifted to 0.0 at the cut-off distance. As expected, this shift did not contribute to the calculation of forces and atom positions, and thus did not affect the results.

## 1.4   Effect of thermostatting

We perform simulations of water droplets transported on the wedge-patterned graphene surface in the (i) NVE ensemble with no thermostatting applied on the water molecules, (ii) NVT ensemble with control of the temperature applied on the overall velocity of the water atoms, (iii) NVT ensemble with the thermostat adjusting only the thermal component of the temperature of the water, calculated only by the peculiar velocities of the particles after subtracting the center-of-mass velocity of the group. From the resulting trajectory of the three cases in Fig. S1, it is clearly shown that the modified NVT gives out the same velocity profile as the non-thermostatted NVE ensemble. This is the setting that was chosen for the rest of the MD simulations, in order to avoid artifacts due to thermostatting.[3,4]
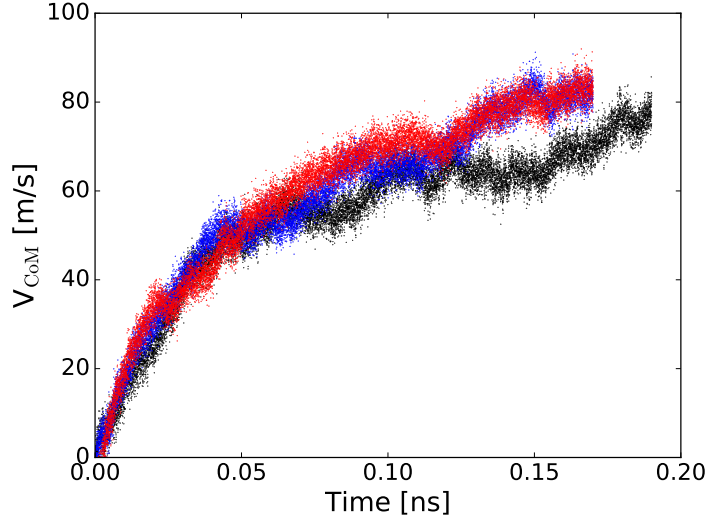
Figure S1: (a) Center-of-Mass (CoM) velocity $V_{CoM}$ *vs.* time for water droplets moving on graphene surfaces with a wedge-shape pattern with the wettabilities listed in Table 2 in the manuscript for different thermostatting options. The graphs extend up to the instant when each droplet reaches the end of the graphene substrate. The red curve corresponds to the NVE ensemble, the black curve to the NVT ensemble and the blue curve to the modified NVT ensemble.

## 1.5   Effect of phonon excitation of the top graphene layer

In the manuscript, the carbon particles remain rigid for all simulations, in order not to perplex the effects of thermal excitation and wettability gradient on the transport of the water droplet. Moreover, in our two-layer graphene, the bottom layer of graphene is expected to act as a solid substrate, constraining the excitation of the top graphene layer. It has been shown before, that, in a system of an equilibrated water-droplet on a double-layer graphene, where the bottom layer remains rigid, the value of the static contact angle shows no deviation between the case where the top graphene layer remains rigid or is allowed to move according to its phonon excitation [5].

In order to check the validity of this assumption, we performed two more simulations of a water droplet on a straight and a wedge-shape patterned graphene sheet, this time allowing the top graphene layer to move freely according to its thermal phonon excitation mode. We observe that the translational motion of the droplet is slightly deteriorated by the graphene vibrations. The end velocity of the water droplet on the graphene surface with the straight

pattern decreases by approximately 8% when the top graphene layer moves due to thermal excitation. On the contrary, the end velocity of the water on the wedge-patterned graphene decreases only by 1.5% when the top graphene sheet is allowed to vibrate (Fig. S2). We believe that the spatial constraint that the wedge pattern imposes on the water droplet results in the observed lower discrepancy between the translational motion of the droplet on the rigid and vibrating graphene.
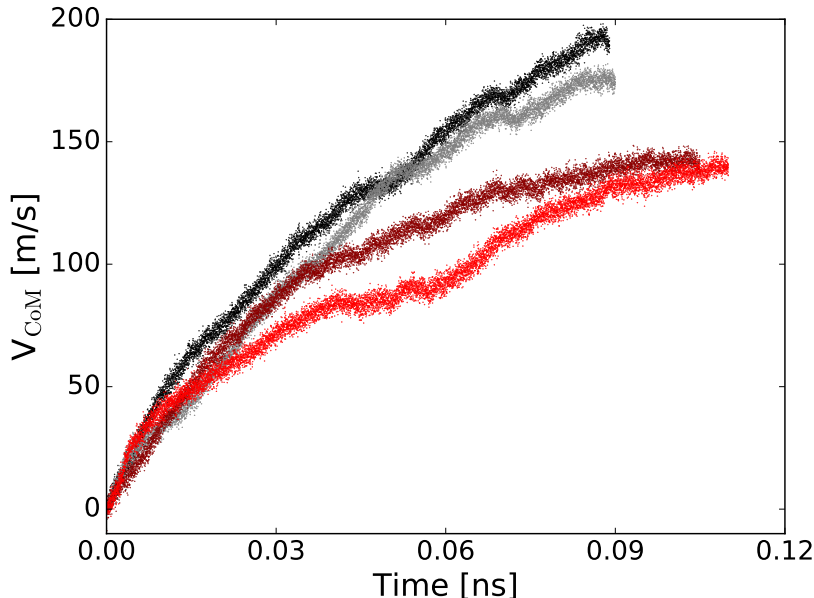


Figure S2: (a) Center-of-Mass (CoM) velocity $V_{CoM}$ *vs.* time for water droplets on a graphene sheet with (i) straight gradient, rigid graphene (black curve), (ii) straight gradient, mobile top graphene (grey curve), (iii) wedge pattern, rigid graphene (dark red curve) and (iv) wedge pattern, mobile top graphene (red curve).

# 2    Simulation Campaign

All MD simulations are summarized in Table S1. Note that pre-production MD equilibrations of the water droplets, as well as the simulations used for the extraction of the friction coefficient, are omitted in this Table. We categorize the various simulation cases according to the following criteria:

- The pattern of the gradient on the graphene surface (straight or wedge).

- The wedge angle $\phi$, when applicable (5°, 10°, 25°).

- The overall maximum gradient of wettability, defined as the difference of the interaction strength of the most hydrophilic zone, $\epsilon_{CO,max}$ and the interaction strength of water with the most hydrophobic zone, $\epsilon_{CO,min}$.

- The droplet equilibrium shape, quantified by the contact angle of the equilibrated droplet $\theta$ ($\theta \approx 95°$ for equilibration over a neutrally wettable surface, $\theta \approx 145°$ for equilibration over a hydrophobic surface, and $\theta = 180°$ for equilibration in vaccum). The values of $\theta$ vary around the proposed values above for different sizes of the equilibrated droplet.

- The size of the droplet, defined through the radius of the contact area of the equilibrated droplet with the surface, $R_{equil}$.

The last column of the Table corresponds to the Section in the manuscript that each simulation case refers to. The numbering of the sections of the main text is hereby declared:

1. Water droplet on two wettability patterns: Uniform gradient *vs.* wedge track

2. Effect of wettability contrast on wedge-track transport

3. Effect of wedge-track angle on nanodroplet transport

4. Effect of initial droplet shape

5. Droplet size effects on wedge-track transport

# 3 Results: Complementary graphs

In this section we present complementary results to those already presented in the main manuscript, mainly graphs of the evolution of the Center-of-Mass (CoM) position, $P_{CoM}$, and velocity $V_{CoM}$ of the droplet for the results sections in the manuscript. The names of the sections and subsections correspond to the respective section names in the main text.

Table S1: MD simulation campaign for transport of nanodroplets on patterned graphene sheets (GRS)

| Case | GRS pattern | $\phi$ [°] | $\epsilon_{CO,max}-\epsilon_{CO,min}$ [kcal/mol] | Equil. $\theta$ [°] | $R_{equil}$ [Å] | manuscript section |
|------|-------------|------------|------------------------------------------|---------------------|-----------------|--------------------|
| 1 | gradient | - | 0.0787 | 95 | 57 | 1 |
| 2 | wedge | 5 | 0.0787 | 95 | 57 | 1 |
| 3 | wedge | 5 | 0.0987 | 95 | 57 | 2 |
| 4 | wedge | 5 | 0.0587 | 95 | 57 | 2 |
| 5 | wedge | 5 | 0.0387 | 95 | 57 | 2 |
| 6 | wedge | 5 | 0.0187 | 95 | 57 | 2 |
| 7 | wedge | 10 | 0.0787 | 95 | 57 | 3 |
| 8 | wedge | 25 | 0.0787 | 95 | 57 | 3 |
| 9 | gradient | - | 0.0787 | 145 | 57 | 4 |
| 10 | wedge | 5 | 0.0787 | 145 | 57 | 4 |
| 11 | gradient | - | 0.0787 | 180 | 57 | 4 |
| 12 | wedge | 5 | 0.0787 | 180 | 57 | 4 |
| 13 | wedge | 1.6 | 0.0787 | 89 | 57 | 5 |
| 14 | wedge | 2.2 | 0.0787 | 96 | 79 | 5 |
| 15 | wedge | 5 | 0.0787 | 94 | 180 | 5 |

## 3.1 Effect of structural variations of the graphene substrate

### 3.1.1 Effect of wettability contrast on wedge-track transport
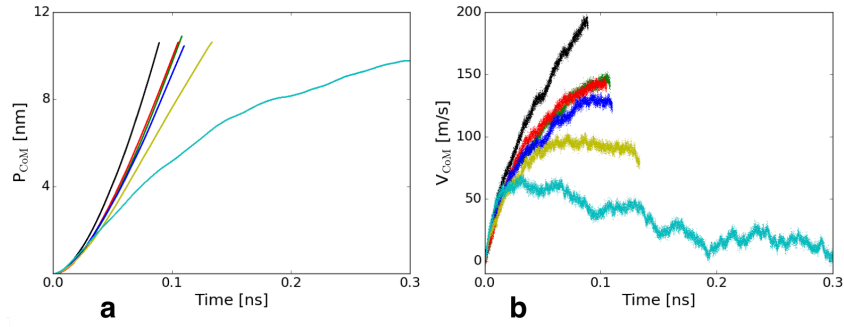


Figure S3: (a) Center-of-Mass (CoM) position $P_{CoM}$, and (b) respective velocity $V_{CoM}$ *vs.* time for water droplets moving on graphene surfaces with a straight wettability gradient pattern and a wedge-shape pattern with the wettabilities listed in Table 2 in the manuscript. The graphs extend up to the instant when each droplet reaches the end of the graphene substrate. Black curves are for the uniform gradient surface; Colored curves refer to different wedge-shaped patterned surfaces, corresponding to the cases listed in Table 2 in the main manuscript: Green curves refer to case 1; Red to case 2; Blue to case 3; Yellow to case 4; Cyan to case 5.

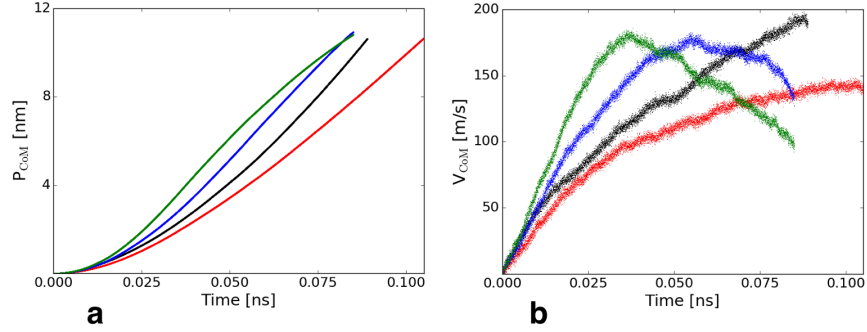### 3.1.2   Effect of wedge-track angle on nanodroplet transport



Figure S4: (a) Center-of-Mass (CoM) position $P_{CoM}$ and (b) respective velocity $V_{CoM}$ *vs.* time for the motion of water droplets on graphene surfaces with a straight gradient wettability pattern and a wedge-shape track with increasing wedge angles $\phi$. The graphs extend up to the instant when each droplet reaches the end of the graphene substrate. Black curves refer to the uniform gradient surface; Colored curves refer to wedge-shaped patterned surfaces, with different wedge angles $\phi$: Red for $\phi = 5°$; Blue for $\phi = 10°$; Green for $\phi = 25°$.

Collecting the results of both of the above subsections, we observe that the hysteresis of contact angle is strongly related to the maximum achieved CoM velocity of the droplet, $V_{CoM}$. In Fig. S5, we plot the maximum hysteresis of the advancing and receding contact angles induced by different wettability gradients *versus* the maximum $V_{CoM}$ of the droplet. We observe that there is a good correlation between the two metrics, which implies that interfacial forces shape the droplet and are subsequently responsible for its rapid motion.
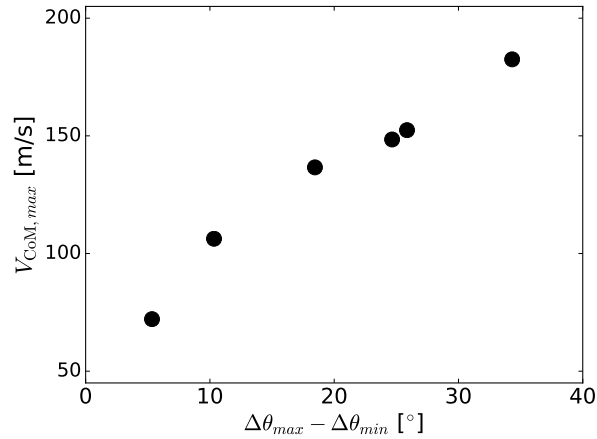


Figure S5:  Relation of maximum difference of hysteresis of contact angles and the maximum achieved velocity of droplets moving on wedge-patterned graphene surfaces.

7

## 3.2 Effect of the droplet shape and size

### 3.2.1 Effect of initial droplet shape

Two droplets, equilibrated on a "neutral" and a superhydrophobic ("phobic") surface, acquire different initial shapes, corresponding to 95° and 144° equilibrium contact angles, respectively. Both droplets follow the same trajectory for the straight and the wedge-track patterns. In Fig. S6, lines in grey tones represent the gradient surface, while those in red tones represent the wedge-patterned surface; Darker shades correspond to the equilibrated "neutral" droplet; lighter shades to the "phobic" droplet. The position of the droplet's CoM ($P_{CoM}$) is shifted to later times for the "phobic" cases, due to the smaller droplet contact area with the surface. The velocities on the gradient surface rise sharply with time, while the corresponding velocities on the wedge pattern level off (Fig. S6b).
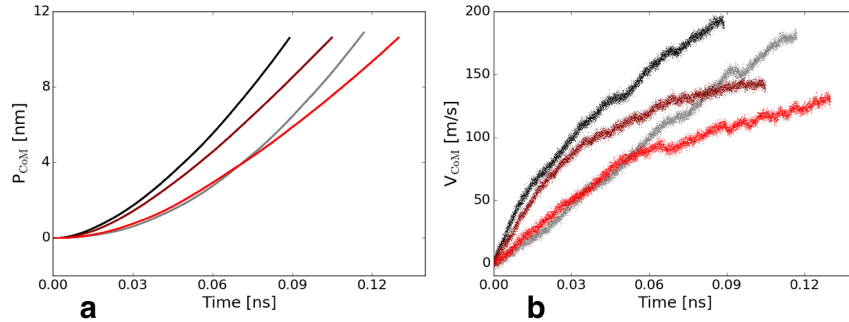


Figure S6: (a) Center-of-Mass (CoM) position $P_{CoM}$, and (b) respective velocity $V_{CoM}$ *vs.* time for water droplets moving on graphene surfaces with a wettability gradient pattern and the wedge-shaped track 2 in Table 2 in the manuscript, using droplets equilibrated on "neutral" and "phobic" surfaces. Black and light grey lines represent the "neutral" and "phobic" droplet cases, respectively, on a uniform gradient surface. Dark red and light red lines represent the "neutral" and "phobic" droplet cases, respectively, on a wedge-patterned surface. The graphs extend up to the instant when each droplet reaches the end of the graphene substrate.

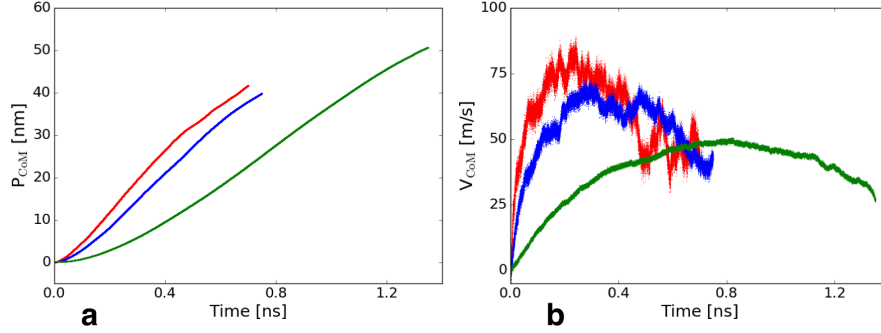### 3.2.2 Droplet size effects on wedge-track transport



**Figure S7:** (a) Center-of-Mass (CoM) position $P_{CoM}$, and (b) corresponding velocity $V_{CoM}$ *vs.* time for the motion of water droplets on the graphene surface with the wedge-shape wettability pattern in case 2 of Table 2 in the main text. The three curves correspond to the three different-sized droplets identified in Table 3 in the main text: Red curves refer to case 1; Blue to case 2; Green to case 3. The graphs extend up to the instant when each droplet reaches the end of the graphene substrate.

# 4 Analytical Force Evaluation

Here, we present in detail the computations leading to an analytical model of the droplet's motion on the wedge-patterned substrate. An instance of the geometry we analyze is shown in Fig. S8. We denote as $(x_0, y_0)$ the starting point of the wedge, where $y_0$ equals half the starting width of the wedge, while $\phi$ is the wedge angle of the pattern. The droplet's center is shown to be at a distance $\delta x$ from the start of the wedge. We denote the two zones of different wettability as follows. The zone with geometric center at $C_B = (x_0 + \delta x, 0)$ and the radius of the surface contact area $r_B$ is the more hydrophilic zone, with contact angle $\theta_B$. The zone with center of curvature at $C_A$ and the radius of the surface contact area $r_A$ is the more hydrophobic zone, with contact angle $\theta_A$. Both zones of the surface are in contact with the water droplet and $\theta_A > \theta_B$.

The motion of the droplet is determined by a driving force ($F_{dr}$) due to difference of wettability across the dividing line segment, $AB$, and by the sum of friction forces ($F_{fr}$) between the water molecules and the substrate on the hydrophilic and hydrophobic zones.
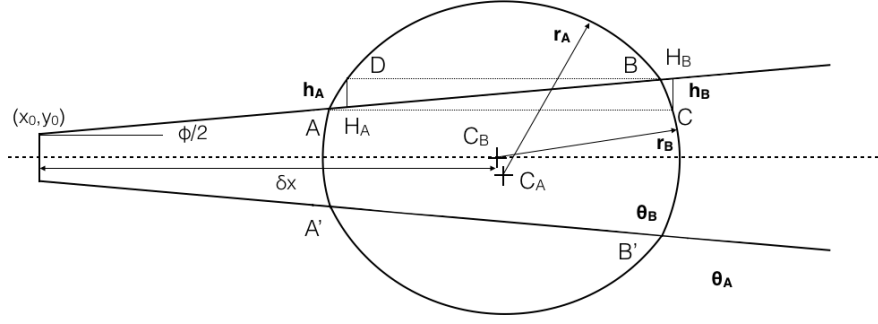
Figure S8: Sketch of the droplet on the patterned substrate. Notation of geometric parameters.

We start by deriving the driving force, $F_{dr}$, which is calculated as: $F_{dr} = 2\gamma A \delta S$, where $\gamma$ is the surface tension for the TIP4P water model in [N/m],[5] $A$ is the contact area of the droplet with the substrate that contributes to the motion actuation in [m$^2$], and $\delta S$ is the difference in wettability between the two zones, calculated as the gradient of wettability in the direction vertical to the line segment AB, $w$, in [m$^{-1}$]. The difference in wettability is only actuating a motion due to the tension on the curved line segment $AB$. This means that the surface area contributing to the droplet's motion is defined as the sum of the areas of the two triangles $ADB$ and $BCA$: $A = A_{ADB} + A_{BCA}$, as the contributions of all other areas cancel each other. The wettability difference in this case is computed as

$$\delta S = \frac{\delta \cos(\theta)}{\delta w} = \frac{\cos(\theta_B) - \cos(\theta_A)}{(h_B + h_A)/2}$$

In order to calculate the triangle areas and the heights $h_A, h_B$, we calculate the moving coordinates of the points: $A, B, C, D, C_A$, knowing that $C_B = (x_0 + \delta x, 0)$ :

$A$ and $B$ are the intersection points of the line segment defined by the wedge and the circle

10

$(C_B, r_B)$. Therefore, $(x_A, y_A)$ and $(x_B, y_B)$ are calculated from the system of equations:

$$\left.\begin{array}{ll} \text{line:} & \frac{y-y_0}{x-x_0} = \tan\left(\phi/2\right) \Longrightarrow y = \tan\left(\phi/2\right)(x - x_0) + y_0 \\[2mm] \text{circle:} & (y-0)^2 + (x - (x_0 + \delta x))^2 = r_B^2 \end{array}\right\}$$

$$\Longrightarrow [\tan\left(\phi/2\right)(x - x_0) + y_0]^2 + [x - (x_0 + \delta x)]^2 = r_B^2$$

This concludes in the following quadratic equation, which is solved for $x$:

$$Ax^2 + Bx + C = 0$$

where:

$$A = \tan^2\left(\phi/2\right) + 1$$

$$B = 2\tan\left(\phi/2\right)y_0 - 2\tan^2\left(\phi/2\right)x_0 - 2(\delta x + x_0)$$

$$C = \tan^2\left(\phi/2\right)x_0^2 + 2\tan\left(\phi/2\right)y_0 x_0 + y_0^2 + (\delta x + x_0)^2 - r_B^2$$

The system is solved for $x_A$ and $x_B$, which are then used to compute $y_A$ and $y_B$ from the circle equation:

$$y_{A,B} = \sqrt{r_B^2 - [x_{A,B} - (x_0 + \delta x)]^2}$$

Continuing, we are now able to compute the coordinates of the center of the circle denoting the radius of the hydrophobic zone, $r_A$, $C_A = (x_{C_A}, y_{C_A})$, since both $A$ and $B$ belong to this circle:

$$(x_A - x_{C_A})^2 + (y_A - y_{C_A})^2 = r_A^2$$

$$(x_B - x_{C_A})^2 + (y_B - y_{C_A})^2 = r_A^2$$

By subtracting the above equations and reordering the terms we deduce:

$$y_{C_A} = -\underbrace{\frac{x_A - x_B}{y_A - y_B}}_{a_y} x_{C_A} + \underbrace{\frac{x_A^2 - x_B^2 + y_A^2 - y_B^2}{2(y_A - y_B)}}_{b_y}$$

Replacing $y_{C_A}$ in one of the above equations, we get the quadratic equation to solve for $x_{C_A}$:

$$A_1 x_{C_A}^2 + B_1 x_{C_A} + C = 0$$

where:

$$A_1 = a_y^2 + 1$$

$$B_1 = 2a_y b_y - 2x_A - 2y_A a_y$$

$$C_1 = x_A^2 + y_A^2 - 2y_A b_y + b_y^2 - r_A^2$$

Then, we can compute the coordinates of the points $C = (x_C, y_C)$ and $D = (x_D, y_D)$ as follows: $C$ belongs to the circle with center $C_B$ and radius $r_B$, whereas $y_C = y_A$:

$$[x_C - (x_0 + \delta x)]^2 + y_C^2 = r_B^2 \implies x_C = (\delta x + x_0) + \sqrt{r_B^2 - y_C^2}$$

$D$ belongs to the circle with center $C_A$ and radius $r_A$, whereas $y_D = y_B$:

$$[x_D - x_{C_A}]^2 + [y_D - y_{C_A}]^2 = r_A^2 \implies x_D = x_{C_A} + \sqrt{r_A^2 - (y_D - y_{C_A})^2}$$

The required $r_A$ and $r_B$ are calculated as the average radii observed for a droplet moving on top of a non-patterned surface with respective contact angles $\theta_A$ and $\theta_B$.

The required heights, $h_A$, $h_B$, are calculated from trigonometric relations of the triangles

12

$H_ADB$ and $ACH_B$. The angles $\widehat{H_BAC}$ and $\widehat{H_ABD}$ are equal to $\phi/2$, thus:

$$h_A = \tan{(\phi/2)}l_{BD}$$

$$h_B = \tan{(\phi/2)}l_{AC}$$

where $l_{BD}$ and $l_{AC}$ are the lengths of the BD and AC line segments respectively.

The contributing surface area $A$ is calculated as the sum of the areas of the triangles $H_ADB$ and $ACH_B$.

Therefore, the driving force due to wettability difference can now be computed in the direction of motion of the droplet, $x$:

$$F_{dr,x} = 2\gamma A\delta S\sin(\phi/2)$$

For the friction force, it is obvious that the more distance the droplet traverses on the wedge-patterned surface, the friction is increased, since the contact area with the more hydrophilic zone also increases. We performed MD simulations of a droplet moving under the influence of a constant applied force on a non-patterned substrate. For varying applied force, the droplet retains a terminal velocity, when the friction force with the surface is opposite and equal to the imposed driving force. We measure the pair force between the surface and the molecules in the first layer of the droplet that is in contact with the substrate and we acquire a relation between the force and the terminal velocity of the droplet. For the range of velocities that interest us ($<150$ m/s) we obtain a friction coefficient for each respective contact angle ($\mu_A$ and $\mu_B$) from linear regression of the resulting data, normalized by the wetting area of the droplet. More on that subject can be found in the section in the manuscript about the friction coefficient.

The friction force in every instance is then comprised of two components, the friction force from the hydrophobic zone and the one from the hydrophilic zone, with each component being calculated as the product of the respective friction coefficient with the underlying contact area and the velocity of the droplet at that position:

$$F_{fr} = (\mu_B A_{AA'B'B} + 2\mu_A A_{\widehat{AB}})U$$

where $AA'B'B$ is the area of the hydrophilic trapezoidal zone defined by AB and their mirrored points, and $\widehat{AB}$ is the circular segment of the hydrophobic zone.

The instantaneous acceleration $\alpha$ in the direction of motion $x$ is computed as:

$$F_{dr,x} - F_{fr} = m\alpha$$

Naturally, zero acceleration indicates when the terminal velocity has been attained.

As shown in the manuscript, from the force evaluation we are able to construct a trajectory of the droplet on the patterned surface analytically, and we find a good agreement for the evolution of the velocity of the droplet along ≈30% of its trajectory, as calculated from the analytical model and the derived velocity evolution from the MD simulations. The simulation and the model results agree for the three droplet sizes described in Table 3 in the main manuscript (Fig. S9).

We expect that the predicted fast pumpless transport of water droplets can be observed in experimental setups. We base this conclusion on calculations we performed, by acquiring approximate values of the geometry, the mass and the initial position and velocity of a droplet on a wedge-patterned surface, as given in Ghosh et al.[6] We extract the following input parameters from Ghosh et al.[6]

- Geometry of the wedge: $\phi = 3°$, initial width $= 0.77$ mm

- Water droplet mass: the water drops were of volume 4.7 $\mu$L. Therefore, the water droplet mass is calculated: $m = \rho V = 997\,\text{kg/m}^3 \cdot 4.7 \times 10^{-9}\,\text{m}^3 \approx 4.686 \times 10^{-6}\,\text{kg}$

- The corresponding diameter of the contact surface of the droplet with the substrate is $D = 2$ mm,

The resulting velocity of a water droplet with the above characteristics from the analytical force evaluation proposed in our manuscript after 150 ms is $V_{\text{CoM,c}} \approx 0.22$ m/s. From Ghosh et al.,[6] Fig.4b, the approximate velocity of the water drops is 0.1 - 0.4 m/s. The two values are in good agreement.
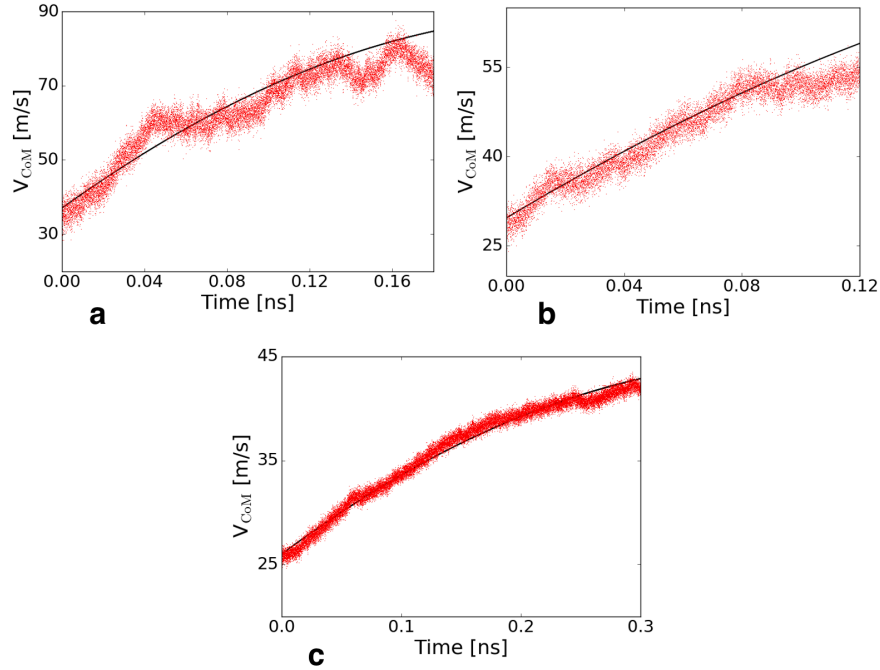


Figure S9: Comparison of the droplet velocity evolution from MD simulations (Red curves) and the analytical model presented in this section (Black curves) for different droplet sizes and geometric features of the substrate scaled accordingly to the droplet size. (a) droplet with $R_{equil} = 57\,\text{Å}$, (b) droplet with $R_{equil} = 79\,\text{Å}$, and (c) droplet with $R_{equil} = 180\,\text{Å}$ (cases 1, 2 and 3 in Table 3 in the main manuscript, respectively).

# References

1. Jorgensen, W. L.; Chandrasekhar, J.; Madura, J. D.; Impey, R. W.; Klein, M. L. Comparison of Simple Potential Functions for Simulating Liquid Water. *J. Chem. Phys.* **1983**, *79*, 926–935.

2. Mayo, S. L.; Olafson, B. D.; Goddard, W. A. DREIDING: A Generic Force Field for Molecular Simulations . *J. Chem. Phys.* **1990**, *94*, 8897–8909.

3. Basconi, J. E.; Shirts, M. R. Effects of Temperature Control Algorithms on Transport Properties and Kinetics in Molecular Dynamics Simulations . *J. Chem. Theory Comput.* **2013**, *9*, 2887–2899.

4. Ruiz-Franco, J.; Rovigatti, L.; Zaccarelli, E. On the Effect of the Thermostat in Non-Equilibrium Molecular Dynamics Simulations . *Eur. Phys. J. E* **2018**, *41*, 80.

5. Alejandre, J.; Chapela, G. A. The Surface Tension of TIP4P/2005 Water Model Using the Ewald Sums for the Dispersion Interactions. *J. Chem. Phys.* **2010**, *132*, 014701.

6. Ghosh, A.; Ranguly, R.; Schutzius, T. M.; Megaridis, C. M. Wettability Patterning for High-Rate, Pumpless Fluid Transport on Open, Non-Planar Microfluidic Platforms. *Lab Chip* **2014**, *14*, 1538–1550.